Journal of Electroanalytical Chemistry 1023 (2026) 120693

Contents lists available at ScienceDirect

Journal of Electroanalytical Chemistry

journal homepage: www.elsevier.com/locate/jelechem

H_2O_2-assisted surface coating of nickel-rich NMC cathodes: Impact of the cathode active material and the niobium source

Valeriu Mereacre [a,*], Yiran Guo [a], Ruochen Xu [a], Markus Weinmann [b], Ralph D. Otterstedt [b], Joachim R. Binder [a]

[a] Institute for Applied Materials – Energy Storage Systems, Karlsruhe Institute of Technology, Eggenstein-Leopoldshafen, 76344, Germany
[b] TANIOBIS GmbH, Goslar, 38642, Germany

ARTICLE INFO

Keywords:
Lithium-ion batteries
NMC811
Layered oxide cathodes
Surface coating
$LiNbO_3$

ABSTRACT

Layered transition metal oxides, particularly those containing nickel, have been widely used as cathode materials and are considered among the most promising options for high-performance lithium-ion batteries. To enhance the cycling and thermal stability of nickel-rich transition metal layered cathodes, surface coating is widely employed in industrial applications. Niobium coating or substitution has shown potential for stabilizing nickel-rich $LiNi_xMn_yCo_zO_2$ (NMC) cathodes. However, its effectiveness is not universal, as pristine commercial materials are often optimized for direct battery use but sometime are unsuitable for further research due to limited processing information. In our efforts to scale up one of our promising coating methods, we initially turned to a commercially available NMC material. However, our attempts to apply the coating method to a commercial NMC were unsuccessful. We attribute this to unknown post-synthesis processing steps used in the commercial product. To circumvent this limitation and properly evaluate our coating technique, we synthesized our own nickel-rich NMC material, NMC811. Electrochemical testing confirmed that the coating method is effective for lab-synthesized NMC materials and also revealed that differences in the Nb precursor composition, despite the same synthesis grade and high nominal purity, significantly influence the resulting electrochemical performance.

1. Introduction

Rechargeable lithium batteries have rapidly emerged as key technologies in the development of green and sustainable energy systems. Today, they are widely used as power sources for electric vehicles and other high-demand applications. Among various cathode materials, layered oxides are considered some of the most promising candidates for high-performance lithium-ion batteries due to their high energy density and structural versatility [1,2]. However, to fully realize their potential, the intrinsic properties of these materials often require optimization. To enhance their electrochemical performance, a variety of experimental strategies have been developed, including elemental doping, morphology control, and surface coating. Due to its excellent ability to facilitate both electron conduction and lithium-ion diffusion, $LiNbO_3$ has been widely employed as a coating material for layered oxide-based cathode materials [3–8]. However, to achieve optimal performance with surface coatings, it is essential to have comprehensive information about the cathode material being modified. This includes detailed knowledge of its structure, composition, and any existing surface modifications, such as coatings or dopants, together with their chemical nature and concentrations. Commercial Ni-rich cathode materials may already contain proprietary surface coatings or other post-synthesis modifications introduced by the manufacturer. Nevertheless, several studies have demonstrated that additional surface coatings or co-coating strategies can further improve the electrochemical performance of such materials [9]. Therefore, knowledge of the surface chemistry and processing history is important for the rational design and interpretation of further surface modification strategies. However, such information is not always disclosed by manufacturers, making it more difficult to establish structure–property relationships and to directly compare results obtained using different commercial materials.

We previously developed a coating method that utilizes hydrogen peroxide (H_2O_2) as an activating agent, achieving excellent results with spinel-type LNMO ($LiNi_{0.5}Mn_{1.5}O_4$) materials [10–12]. This approach significantly shortened the reaction time and promoted uniform deposition of various coating layers, leading to improved surface stability and

* Corresponding author.
E-mail address: valeriu.mereacre@kit.edu (V. Mereacre).

https://doi.org/10.1016/j.jelechem.2026.120693
Received 20 August 2026; Received in revised form 9 October 2026; Accepted 15 October 2026
Available online 17 October 2026
1572-6657/© 2026 The Authors. Published by Elsevier B.V. This is an open access article under the CC BY license (http://creativecommons.org/licenses/by/4.0/).
Open access funding enabled and organized by Projekt DEAL.

enhanced electrochemical performance. Given these advantages, we hypothesized that the method could also be effectively applied to layered oxide cathodes such as NMC ($LiNi_xMn_yCo_zO_2$). To facilitate scaling up the method, we required large quantities of active material and therefore acquired a commercial single-crystal NMC, $LiNi_{0.82}Mn_{0.07}Co_{0.11}O_2$ (Ni82), from MSE Supplies, which reported >80% capacity retention after 1500 cycles at 1C. In addition, single-crystal NMC materials are generally regarded as structurally more stable and are considered promising candidates for long-lifetime EV applications. However, even materials with excellent baseline performance can often be further optimized. This was the motivation behind our work - to improve an already high-performing material. In this study, we applied a $LiNbO_3$ coating to Ni82, aiming to enhance its interfacial stability and overall electrochemical performance. $LiNbO_3$ is well known for its ability to facilitate both electronic conductivity and lithium-ion transport, and has therefore been widely used as a surface modifier for layered oxide cathodes [10–15]. Despite this, our efforts to apply a $LiNbO_3$ coating to the Ni82 material yielded unexpected and disappointing results. Specifically, we observed lower specific capacity, poor cycling stability, and generally catastrophic electrochemical performance.

The unexpectedly poor electrochemical performance of the $LiNbO_3$-coated commercial Ni82 material using H_2O_2 stood in sharp contrast to the promising results previously obtained with spinel cathodes [10–12], prompting a closer examination of the coating method. To determine whether the observed failure was specific to the commercial Ni82 material or inherent to the H_2O_2-assisted coating process itself, we synthesized layered $LiNi_{0.8}Mn_{0.1}Co_{0.1}O_2$ (NMC811) using two different synthesis routes. NMC811 was deliberately selected instead of self-synthesized Ni82 because it is one of the most extensively studied nickel-rich layered oxides, allowing direct comparison of our results with a large body of published literature. In contrast, only a limited number of studies are available for Ni82, making a meaningful comparison considerably more difficult. Although the nickel content differs by only 2 mol% (80% vs. 82%), both materials belong to the same family of Ni-rich layered oxides and are often considered part of the Ni80+ class of cathode materials. Consequently, they exhibit very similar structural and electrochemical characteristics, making such a comparison scientifically justified.

The synthesized NMC811 powders were coated with Li/Nb oxides using niobium ethoxide precursors from two suppliers following exactly the same H_2O_2-assisted coating procedure that had previously failed for the commercial Ni82 material. The coated samples were subsequently characterized by electrochemical testing, X-ray photoelectron spectroscopy (XPS), scanning electron microscopy (SEM), and X-ray diffraction (XRD). In contrast to commercial Ni82, both NMC811 systems exhibited improved electrochemical performance after coating, demonstrating that the H_2O_2-assisted coating strategy itself is effective. These findings indicate that the poor performance observed for commercial Ni82 is not an intrinsic limitation of the coating method but is instead likely related to the unknown processing history and proprietary post-synthesis treatments of the commercial material. While recognizing the differences in initial morphology, composition, and surface states between these host matrices, evaluating them side-by-side is highly justified within the Ni80+ class. This comparison serves to expose a critical practical issue: how undisclosed commercial pre-treatments can directly dictate the success or failure of subsequent coating reactions. The origin of this contrasting behavior is discussed in detail in the following sections.

2. Experimental section

2.1. Synthesis of cathode active material

Commercial single-crystal $LiNi_{0.82}Mn_{0.07}Co_{0.11}O_2$ (Ni82) was acquired from MSE Supplies. The synthesis of NMC811 was carried out in two main steps. First, the $Ni_{0.8}Mn_{0.1}Co_{0.1}(OH)_2$ precursor was synthesized via a conventional coprecipitation method in a continuously stirred tank reactor, following a procedure similar to that described by Van Bommel et al. [16] In the second step, the obtained hydroxide precursor was thoroughly mixed with a stoichiometric amount of either Li_2CO_3 or LiOH and subsequently calcined in an oxygen atmosphere. The thermal treatment involved an initial heating at 250 °C for 2 h, followed by calcination at either 800 °C or 775 °C for 5 h at a heating rate of 4 °C/min. The samples were then cooled to room temperature at a rate of 2 °C/min. The resulting materials were designated as NMC811C (Li_2CO_3 route) and NMC811H (LiOH route), respectively. For comparison, reference samples NMC811C-350 and NMC811H-350 were prepared by calcining the same precursors at 350 °C in O_2, using the same heating and cooling program.

The choice of 800 °C for the Li_2CO_3-based route and 775 °C for the LiOH-based route reflects the different thermal behaviors and reactivities of the lithium sources: LiOH decomposes and becomes reactive at lower temperature than Li_2CO_3, enabling sufficient lithiation and crystallization at a slightly lower sintering temperature and reducing Li-loss; Li_2CO_3, being more thermally stable, typically requires a higher final temperature to ensure full reaction, crystallinity, and reduced cation mixing [17–19]. These temperatures represent standard, optimized conditions for each specific lithium precursor in literature. Using identical temperatures for both would result in either incomplete reaction for the carbonate or high lithium loss for the hydroxide, preventing a fair comparison.

2.2. Surface coating via a H_2O_2-chemistry approach

A lithium niobium oxide $LiNbO_3$-based surface coating was applied to Ni82, NMC811C, and NMC811H cathode materials using a solution-based chemical method involving H_2O_2 as an activating agent, in accordance with our previously reported procedure [20].

To prepare the Li/Nb coating solution, 0.30 g (0.94 mmol) of niobium(V) ethoxide (either Aldrich (**A**) or TANiOBIS (**T**), both synthesis grade, high purity) was dissolved in 20 mL of absolute ethanol, while 0.057 g (1.08 mmol) of lithium ethoxide (Aldrich) was separately dissolved in 40 mL of absolute ethanol. The two solutions were then combined, followed by the addition of 60 mL of 30% hydrogen peroxide and ~ 0.1 mL (8 drops) of 65% nitric acid (HNO_3). The resulting mixture was stirred until a clear solution was obtained, indicating complete dissolution of the precursors.

To coat Ni82, NMC811C, and NMC811H with 0.5 wt% $LiNbO_3$, 1.2 g of the respective cathode active material and 13 mL of absolute ethanol were added to a round-bottom flask (V = 50 mL). The resulting suspension was stirred for approximately 3 min before 5.2 mL of the Li/Nb coating solution (corresponding to ~0.5 wt% $LiNbO_3$), prepared using niobium(V) ethoxide (A or T), was added dropwise under continuous stirring. Stirring was continued until gas evolution ceased (approximately 25 min). The suspension was then decanted, and the powder was washed with ethanol, centrifuged, dried at 80 °C, and calcined in oxygen first at 250 °C for 2 h, followed by 350 °C for 5 h at a heating rate of 4 °C/min. The samples were subsequently cooled to room temperature at a rate of 2 °C/min.

Uncoated samples (Ni82, NMC811C, and NMC811H) were calcined under the same conditions and in the same oven as the coated samples to ensure comparability. Samples were labeled as follows: Ni82, Ni82–350, and Ni82-LN-E-350 (LN = $LiNbO_3$, E = Ethanol). Self-synthesized samples were labeled as follows: for the Li_2CO_3 route – NMC811C, NMC811C-350, NMC811C-LN(A)-350, and NMC811C-LN(T)-350; for the LiOH route – NMC811H, NMC811H-350, NMC811H-LN(A)-350, and NMC811H-LN(T)-350. Here, LN(A) and LN(T) refer to $LiNbO_3$ coatings using the Nb(V) precursor A and T, respectively. All coated and uncoated materials were stored in a glovebox.

Since Ni82 is the most sensitive to the reaction conditions, a test coating experiment was conducted using water instead of ethanol. The

material was coated with 0.5 wt% $LiNbO_3$ via an aqueous route, using lithium acetate and ammonium niobium oxalate (NbAmOx, $NH_4[Nb(O)(C_2O_4)_2(H_2O)_2]\cdot 3H_2O$) as precursors, both dissolved in water. The Li/Nb (W) solution was prepared as follows: 0.35 g (3.43 mmol) of $LiO_2CCH_3\cdot 2H_2O$ was dissolved in 10 mL of water, and 1.32 g (3.35 mmol) of NbAmOx was separately dissolved in 20 mL of water. The two solutions were then combined, followed by the addition of 30 mL of 30% H_2O_2 and approximately 0.1 mL (8 drops) of 65% HNO_3.

To coat Ni82 with ~0.5 wt% $LiNbO_3$, 5.4 g of Ni82 and 75 mL of water were added to a 250 mL round-bottom flask. The resulting suspension was stirred for approximately 3 min before 3.2 mL of the Li/Nb (W) coating solution was added dropwise under continuous stirring. Stirring was continued until gas evolution finished (approximately 6 h). The suspension was then decanted, and the powder was washed with water, centrifuged, and dried at 80 °C.

Additionally, uncoated Ni82 was treated with water and with diluted (~7%) H_2O_2 (under similar conditions but without Li/Nb precursors) to evaluate whether these solvents affect the electrochemical behavior of Ni82. After synthesis, all three materials were calcined at 350 °C under the same conditions as the other samples. The samples were labeled as Ni82-LN-W-350, Ni82-H_2O-350, and Ni82-H_2O_2–350, respectively. Analogous to Ni82-LN-W-350, an aqueous coating reaction was also performed for NMC811C, yielding the sample NMC811C-LN-W-350.

2.3. Material characterization

A scanning electron microscope SEM (Zeiss Supra 55) was used to analyze the morphology. Powder X-ray diffraction was recorded using a Bruker D2 Phaser Diffractometer with Cu-K_α radiation ($\lambda = 1.5406$ Å) and a LynxEye XE-T detector in reflection mode. XRD patterns were recorded over a 2θ range of 10–80°/90° with step size of 0.02° and counting time of 1 or 2 s per step. Rietveld refinements were performed on TOPAS-V6 (Bruker AXS) and software jEdit.

2.4. Electrochemistry

Electrochemical testing of the materials coated with 0.5 wt% $LiNbO_3$ was conducted following previously established protocols. Electrode slurries were prepared using a composition of 80 wt% active material, 10 wt% Super C carbon black, and 10 wt% polyvinylidene fluoride (PVDF), with *N*-methyl-2-pyrrolidone (NMP) serving as the solvent. The resulting slurry was cast onto aluminum foil and dried 24 h at 80 °C before cell assembly. The average active material mass loading of the electrodes was approximately 4.1 mg cm^{-2}, with an electrode area of 1.13 cm^2. Coin-type half-cells (CR2032) were assembled in an argon-filled glovebox. Lithium metal foil (12 mm diameter, 25 μm thickness) was used as the counter electrode, and Celgard 2325 (Celgard, Sélestat, France) served as the separator. The electrolyte consisted of 210 μL of commercial LP30 (1.0 M LiPF6 dissolved in a 50:50 wt% mixture of ethylene carbonate (EC) and dimethyl carbonate (DMC)). Galvanostatic cycling was carried out at 23 °C within a voltage window of 3.0–4.3 V vs. Li^+/Li. The first cycle was performed at a C/20 rate, followed by two cycles at C/10. Subsequent cycling was conducted at a charge rate of C/2 and a discharge rate of 1C to evaluate long-term performance, where the 1C rate is defined based on a theoretical specific capacity of 220.4 $mAhg^{-1}$. To ensure reproducibility, 3 replicate cells were fabricated and tested for each sample group. The figures display representative curves, showing consistent electrochemical trends with typical cell-to-cell capacity variations of approximately 4 $mAhg^{-1}$.

2.5. Elemental analysis

Elemental analysis (EA) was done at the IAM-AWP, Chemical analysis laboratory, KIT, using inductively coupled plasma optical emission spectrometry (ICP-OES, iCAP 7600 DUO, Thermo Fisher Scientific GmbH, Dreieich, Germany) to determine the Li, Ni, Co, Mn, O and Nb elements.(Table S1).

2.6. X-ray photoelectron spectroscopy

XPS measurements were performed using a K-Alpha+ XPS spectrometer (ThermoFisher Scientific, East Grinstead, UK). Data acquisition and processing were conducted with the Thermo Avantage software. All powders were analyzed using a microfocused, monochromated Al Kα X-ray source (400 μm spot size). The K-Alpha+ charge compensation system was employed during analysis, using electrons of 8 eV energy, and low-energy argon ions to prevent any localized charge build-up.

3. Results and discussion

As mentioned in the Introduction, to build on our earlier success with a H_2O_2-based coating method, previously shown to be highly effective for spinel-type LNMO ($LiNi_{0.5}Mn_{1.5}O_4$) materials [10–12], we sought to extend this approach to layered NMC materials and explore its scalability. As an initial step toward upscaling, we selected a commercially available NMC material. However, applying the coating method to the commercial NMC proved unsuccessful. We suspect this outcome is due to undisclosed post-synthesis treatments commonly applied by manufacturers, which may interfere with the coating process. To overcome this issue and enable a proper evaluation of the technique, we proceeded to synthesize our own nickel-rich NMC811 material. This composition was selected because NMC811 is the most widely studied Ni-rich layered oxide in the context of Li/Nb-based surface coatings [3,7,21].

3.1. Morphological characterization

Fig. 1 presents scanning electron microscopy (SEM) images of the commercial, single crystal layered oxide material Ni82 (Fig. 1, a) and two self-synthesized NMC811 ($LiNi_{0.8}Mn_{0.1}Co_{0.1}O_2$) samples prepared via different lithium sources: Li_2CO_3 (Fig. 1, b) and LiOH (Fig. 1, c). The commercial Ni82 sample exhibits well-faceted, polyhedral primary particles with a dense and compact microstructure. The particle surfaces appear relatively smooth, indicating high crystallinity (also confirmed by X-Ray diffraction, vide infra). The average particle size ranges from approximately 300 to 1600 nm. The large, uniform grains and clean grain boundaries are indicative of a well-developed layered structure, typically associated with solid-state synthesis routes and high-temperature calcination.

In contrast, the self-synthesized NMC811C materials show distinctly different morphologies. The sample synthesized via the Li_2CO_3 route displays agglomerated, sub-micron-sized primary particles with irregular shapes and a rougher surface texture. A qualitative, visually derived particle size distribution indicates a much narrower range compared to the commercial sample, with primary particles visually estimated to be roughly 300 nm. The agglomerates form a porous network, which could be beneficial for lithium-ion diffusion due to increased surface area.

The NMC811H sample synthesized using the LiOH route shows an even more porous and loosely agglomerated structure. The primary particles are smaller and more spherical compared to the Li_2CO_3-derived sample, with dimensions generally below 200 nm. The high degree of agglomeration and the pronounced porosity observed in this sample may arise from differences in the thermal decomposition behavior of LiOH compared to Li_2CO_3 during the synthesis process. Using LiOH as the lithium precursor leads to faster reactions, which can result in lithium loss and cation mixing [22] (proved by XRD, vide infra) at high temperatures. This morphology suggests a potentially higher specific surface area, which may enhance electrochemical reactivity but could also increase side reactions with the electrolyte.

3.2. Structural characterization via X-ray diffraction

X-ray diffraction (XRD) is typically the initial characterization

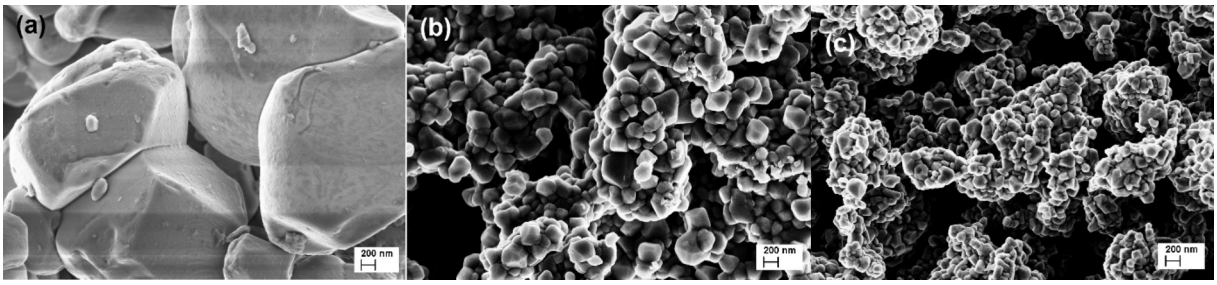


Fig. 1. SEM images of the commercial Ni82 (a) and self-synthesized NMC811C (Li_2CO_3 route) (b) and NMC811H (LiOH route) (c) cathode materials.

technique employed when a new material, such as a cathode material, is synthesized. This approach ensures that the crystal structure corresponds to the expected phase, as proceeding with further analysis is not meaningful if structural integrity is not confirmed.

Fig. 2 displays the X-ray diffraction (XRD) patterns of the commercial Ni82 sample (top, blue) and the two self-synthesized NMC811 materials prepared via the Li_2CO_3 (NMC811C, middle, red) and LiOH (NMC811H, bottom, black) routes. All samples exhibit diffraction peaks characteristic of a layered α-$NaFeO_2$-type structure with a rhombohedral (R-3 m) space group, commonly found in Ni-rich layered oxides.

The commercial Ni82 material shows sharp and well-defined diffraction peaks, indicating high crystallinity and a well-ordered *R-3 m* layered structure. The clear splitting of the (006)/(012) and (108)/(110) peaks is especially noteworthy, as this is a reliable indicator of good phase purity and low cation mixing between Li^+ and Ni^{2+} in the structure. Such peak splitting is widely used as an indicator of good structural ordering in Ni-rich layered oxides [23,24]. The strong intensity ratio of the (003)/(104) reflections further supports a well-developed layered structure with minimal Ni^{2+} migration into the Li layers (~3.4%) (Fig. S1).

In comparison, both self-synthesized NMC811 samples also exhibit the typical reflections of the layered structure, but with notable differences in peak sharpness and resolution. The NMC811C sample displays slightly broader peaks than the commercial sample, suggesting smaller coherent crystallite sizes or minor structural disorder. While the peak splitting at (006)/(012) and (108)/(110) is still observable, it is less pronounced, indicating smaller crystallite sizes, a moderate degree of cation mixing (~6.7%) (Fig. S1) and/or slightly lower structural ordering than the commercial counterpart. This may reflect the fact that synthesis using Li_2CO_3 often requires higher temperatures and longer calcination times, and if these conditions are not fully optimized, it can lead to slight compositional inhomogeneity or incomplete structural ordering.

The NMC811H sample shows the broadest peaks among the three, with less distinct separation between the (006)/(012) and (108)/(110) reflection pairs. This broadening implies a further reduction in crystallite size and/or local disorder/cation mixing, consistent with the highly agglomerated, nanostructured morphology observed in SEM (Fig. 1). The diminished (003)/(104) intensity ratio suggests increased cation mixing (~8.8%), which can impede lithium-ion diffusion and negatively impact electrochemical performance, and this is corroborated by the electrochemical measurements (vide infra): the electrochemistry for these two pristine materials, meaning they were only once calcined at 775 and 800 °C, respectively, shows that the NMC811H compound exhibits a much smaller initial capacity and much faster degradation. Only after a second calcination at 350 °C (NMC811H-350) does the cation mixing decrease (~5.1%) (Fig. S2 and S3), and the electrochemistry becomes nearly identical to that of NMC811C-350 (vide infra, Fig. 5). This is likely a result of the more reactive LiOH precursor, which may induce rapid phase formation and insufficient atomic ordering during synthesis, as evidenced by in-situ studies showing that lithiation proceeds faster with $LiOH{\cdot}H_2O$ than with Li2CO3 [25].

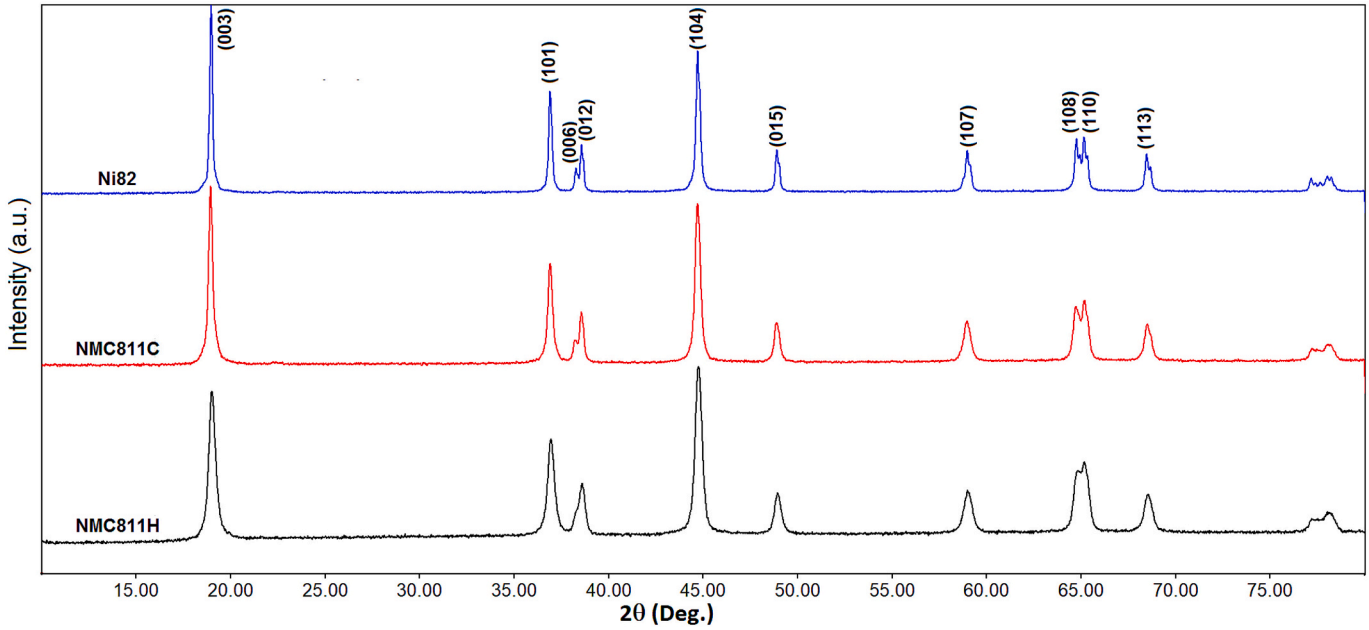


Fig. 2. XRD patterns for commercial Ni82 and self-synthesized NMC811C (Li_2CO_3 route), and NMC811H (LiOH route). Rietveld refinement analysis is presented in SI (Fig. S1).

These structural findings are in good agreement with the SEM observations. The commercial Ni82 sample, with its large, well-formed crystals, exhibits a high degree of structural order and crystallinity. In contrast, the self-synthesized NMC811 samples, particularly the LiOH-derived variant, show smaller, more agglomerated particles and correspondingly lower crystallinity and layered ordering. Such structural and morphological differences are expected to influence the electrochemical behavior, particularly in terms of capacity retention and stability.

3.3. Electrochemical testing of Ni82 electrodes

As an initial step in evaluating the electrochemical performance of the three materials, we investigated Ni82 as the active material for positive electrodes. Electrodes were first prepared using the pristine Ni82 powder without any additional treatment. Subsequently, the same material was subjected to calcination at 350 °C, and electrodes were again fabricated under identical conditions. The choice of 350 °C as the calcination temperature is deliberate, as this temperature is employed in the subsequent coating procedure using $LiNbO_3$. According to the literature, calcination at 350 °C results in the formation of an amorphous $LiNbO_3$ layer, which has been shown to yield optimal electrochemical performance [20,26].

The Fig. 3 compares the electrochemical behavior of bare Ni82 (black), thermally treated Ni82 at 350 °C (Ni82–350, blue), and Ni82 coated with 0.5 wt% $LiNbO_3$ and calcined at 350 °C (Ni82-LN-E-350, green). The initial discharge capacities were 182.5, 173.2, and 146.4 mAh g^{-1}, respectively. The slight reduction in initial capacity observed for Ni82–350 compared to pristine Ni82 may be attributed to subtle structural degradation induced by the thermal treatment, despite 350 °C being a relatively mild annealing temperature. Both the pristine and thermally treated samples show a comparable trend of gradual capacity fading over 400 cycles.

In contrast, the coated sample Ni82-LN-E-350 exhibits a noticeably different behavior. After the first few cycles, a rapid drop in capacity is observed, falling to ~70.1 mAh g^{-1} by the third cycle. A minor recovery is noted around cycle 40, followed by a continued decline. This unexpected performance degradation suggests an adverse interaction between the coating and the Ni-rich NMC surface under the applied conditions, contrary to the typical improvement seen with $LiNbO_3$ coatings in similar systems [3–8].

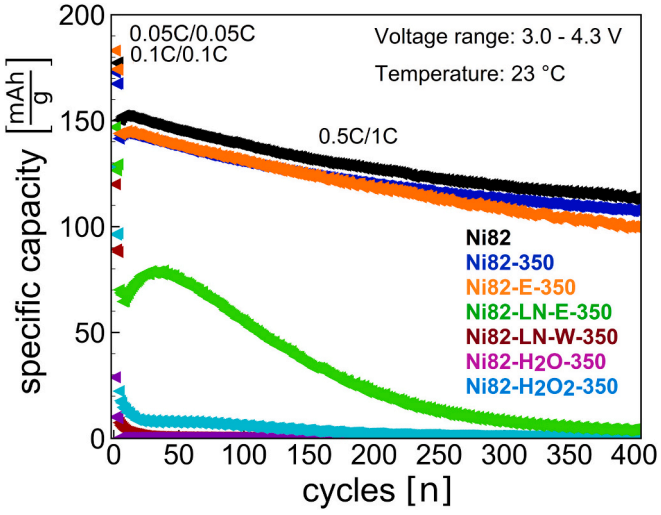


Fig. 3. Cycling performance of various Ni82-based electrodes at a 1C rate (after one initial formation cycle at 0.05C and two at 0.1C): bare Ni82 (black), thermally treated Ni82 at 350 °C (Ni82–350, blue), and Ni82 coated with 0.5 wt % $LiNbO_3$ (Nb-ethoxide)/Ethanol route) (Ni82-LN-E-350, green), Ni82 coated with 0.5 wt% $LiNbO_3$ (NbAmOx/Water route) (Ni82-LN-W-350, brown), Ni82 treated with H_2O (Ni82-H_2O-350, violet), Ni82 treated with Ethanol (Ni82-E-350, orange) and Ni82 treated with H_2O_2 (Ni82-H_2O_2–350, turquoise), all being calcined at 350 °C. (For interpretation of the references to colour in this figure legend, the reader is referred to the web version of this article.)

To further investigate the influence of solvents used in the coating reactions, a 0.5 wt% $LiNbO_3$-coated Ni82 sample was prepared using NbAmOx as a precursor in water (Ni82-LN-W-350, brown). However, this approach resulted in an even more severe capacity loss, indicating a complete failure of electrochemical activity. Additional tests with Ni82 samples treated only with H_2O, diluted H_2O_2, or Ethanol, Ni82-H_2O-350 (violet), Ni82-H_2O_2–350 (turquoise) and (Ni82-E-350 (orange), respectively, also exhibited poor performance, suggesting that surface modification caused by these solvents may be detrimental.

These findings are somewhat surprising, considering that this material is generally regarded as suitable for direct use in batteries. It seems that it is stable when it comes in contact with common battery electrolytes and has most probably undergone extensive factory testing. However, our results indicate that while the material performs well under standard conditions, its surface is highly sensitive to contact with certain solvents, specifically H_2O, H_2O_2, or ethanol, during processing steps such as coating. Even brief exposure during these treatments can induce surface degradation, ultimately altering the electrochemical behavior of the cathode active material, despite subsequent coating, drying, and calcination steps.

This interpretation is further complicated by the limited information typically available for commercial cathode materials. While manufacturers generally provide the nominal composition and, in some cases, information on the presence of dopants or surface modifications, detailed information about their chemical nature and processing history is often not available. For the commercial Ni82 material investigated in this study, the supplier indicated the presence of Zr as a dopant and a Zr/B surface coating. However, this description does not specify the chemical form of these species. For example, it remains unclear whether boron is present as a borate, whether zirconium exists as an oxide or another compound, or whether both elements are incorporated into a single phase. Similarly, no information is available regarding the crystallinity of the coating, its thickness, the coating process, or the thermal treatments applied during manufacturing. Such details are important for understanding how subsequent surface modifications interact with the original material and for interpreting the resulting electrochemical behavior.

As mentioned above, to overcome these limitations, we synthesized our own cathode material, $LiNi_{0.8}Mn_{0.1}Co_{0.1}O_2$ (NMC811), using two different synthetic routes based on Li_2CO_3 and LiOH. For both NMC811 variants, a single coating procedure was applied using Li/Nb precursors dissolved in ethanol (under the same conditions as for Ni82), with niobium ethoxide obtained from two suppliers. The use of precursors with different purity grades (p.a. and technical grade) also enabled evaluation of the influence of precursor quality on the coating process and the resulting electrochemical performance. This approach, using Li/Nb precursors dissolved in ethanol, is frequently reported in the literature for studies involving Li/Nb-based surface coatings such as $LiNbO_3$ [3,7,21]. Unlike for the commercial Ni82 sample, no detailed variations in solvent systems were investigated for the self-synthesized materials in this work, as such studies have already been extensively reported in the literature [27]. Only for NMC811C, which exhibited a better-defined layered structure, an analogous aqueous coating reaction using NbAmOx was performed, resulting in the sample NMC811C-LN-W-350 (Fig. S4).

3.4. Electrochemical testing of NMC811 electrodes

The cycling performance of the carbonate-based samples is presented in Fig. 4. The pristine NMC811C (black) exhibits moderate capacity retention over 400 cycles at 0.5C/1C. Thermal treatment at 350 °C (NMC811C-350, blue) results in a slight reduction in specific capacity and cycling stability, possibly due to surface densification or Li loss

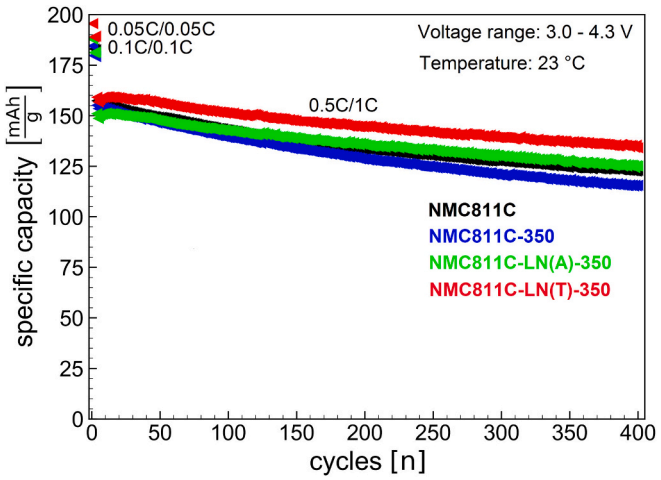


Fig. 4. Specific capacity vs. cycle number for NMC811 cathode materials synthesized using Li_2CO_3 as the lithium source. Samples include uncoated NMC811C (black), thermally treated NMC811C-350 (blue), $LiNbO_3$-coated NMC811C-LN(A)-350 (green) using A-Nb-precursor, and NMC811C-LN(T)-350 (red) using T-Nb-precursor. All coated samples contain 0.5 wt% $LiNbO_3$ and were calcined at 350 °C. Testing was conducted at 0.5C/1C (after one initial formation cycle at 0.05C and two at 0.1C) in a voltage window of 3.0–4.3 V at 23 °C. (For interpretation of the references to colour in this figure legend, the reader is referred to the web version of this article.)

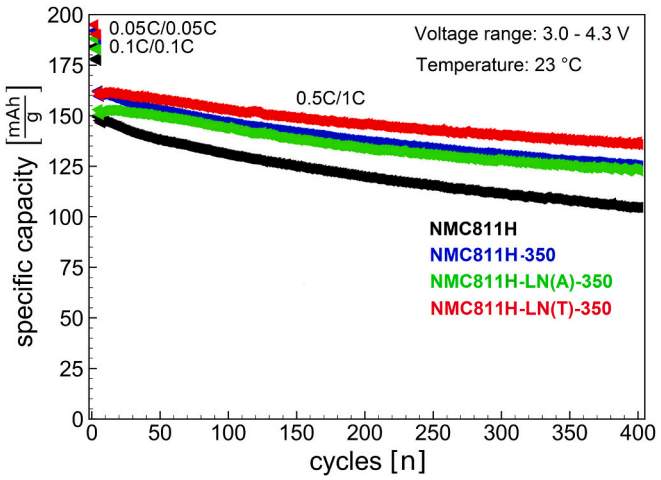


Fig. 5. Specific capacity vs. cycle number for NMC811 cathode materials synthesized using LiOH as the lithium source. Samples include uncoated NMC811H (black), thermally treated NMC811H-350 (blue), $LiNbO_3$-coated NMC811H-LN(A)-350 (green) using A-Nb-precursor, and NMC811H-LN(T)-350 (red) using T-Nb-precursor. All coated samples contain 0.5 wt% $LiNbO_3$ and were calcined at 350 °C. Testing was conducted at 0.5C/1C (after one initial formation cycle at 0.05C and two at 0.1C) in a voltage window of 3.0–4.3 V at 23 °C. (For interpretation of the references to colour in this figure legend, the reader is referred to the web version of this article.)

during calcination.

Surface coating with $LiNbO_3$ significantly improves electrochemical performance. The A-derived coating (NMC811C-LN(A)-350, green) offers improved capacity retention compared to uncoated samples. Notably, the T-derived coating (NMC811C-LN(T)-350, red) outperforms all other variants, showing the highest specific capacity and a modest improvement in capacity retention, suggesting a superior coating uniformity or reactivity of the T-precursor. This result highlights the critical influence of Nb-precursor chemistry on coating effectiveness and electrochemical stability.

Given the better defined layered structure of NMC811C, an additional aqueous coating step using NbAmOx was performed, resulting in the sample NMC811C-LN-W-350. However, the electrochemical performance was poor (Fig. S4), indicating that self-synthesized nickel-rich NMC811 materials (similar to Ni82) are also highly sensitive to water, and that successful coating of such materials using H_2O_2-method can only be achieved via the ethanol-based route, despite the presence of water in the H_2O_2 used for this process. Although the aqueous route uses a different precursor (NbAmOx) and longer reaction times, the primary reason for the poor performance is the well-known water sensitivity of Ni-rich host matrices, which leads to severe lithium leaching. Our H_2O_2-assisted method itself is robust, as proven by cross-sectional TEM on similar systems in our recent work [20]. The failure on commercial Ni82 is caused by the interaction with the unknown pre-existing surface layer rather than a failure of the coating method.

Fig. 5 displays the cycling performance of the LiOH-based NMC811H samples. The unmodified NMC811H (black) demonstrates the lowest capacity retention among all samples, indicative of inferior surface stability or structural degradation possibly induced by residual lithium compounds or greater Li/Ni cation mixing typically associated with LiOH-based synthesis.

Thermal treatment (NMC811H-350, blue) markedly improves performance but remains inferior to coated samples. Coating with $LiNbO_3$ again shows enhancement in electrochemical behavior. Similar to the carbonate-based series, the T-coated sample (NMC811H-LN(T)-350, red) delivers the best performance among the LiOH-derived materials, both in terms of initial capacity and cycling stability, confirming the consistency of the T-precursor's effectiveness across different synthesis routes. It also appears that the Li/Nb coating can reduce the degree of polarization associated with the redox reactions. It is noteworthy that, although this effect is not clearly pronounced for NMC811C, it is clearly observable for NMC811H (Figs. S6,S7). After 400 cycles, the potential differences between the redox peaks of the coated samples (~0.078–0.085 V) were smaller than those of the pristine (~0.142 V) and pristine-calcined (~0.155 V) electrodes. This clear difference in peak separation demonstrates that the coated samples possess enhanced electrochemical stability and reversibility.

Interestingly to mention that Li/Ni cation mixing is clearly visible in the XRD patterns of the unmodified sample (NMC811H) (Fig. 2), and is notably reduced after calcination at 350 °C (see NMC811H-350, Figs. S2, S3). This suggests that an additional thermal treatment at 350 °C for the LiOH-based NMC811 samples leads to beneficial changes in their electrochemical performance. Moreover, although carried out at a relatively low temperature, this thermal treatment appears to induce significant structural modifications, as supported by the XRD data: for example, the sharper (006)/(012) reflections and the increased (003)/(104) intensity ratio indicate a better-developed layered structure with a much lower degree of cation mixing (NMC811H (8.8%) - > NMC811H-350 (5.1%)). Therefore, the improved capacity observed in the coated and thermally treated NMC811H samples is likely due not only to the presence of the Li/Nb coating, but also to the structural effects of the 350 °C treatment. The extent of cation disorder reduction achieved at this modest temperature is unexpectedly high, as such substantial changes are typically associated with higher-temperature processes. In contrast, for the commercial Ni82 material, the same 350 °C treatment results in a slight decline in electrochemical performance (Fig. 3). This indicates that for certain commercial NMC materials, even mild post-synthesis thermal treatments can be detrimental.

3.5. Comparative analysis

Across both synthesis routes, $LiNbO_3$ surface modification clearly improves long-term cycling stability and specific capacity. The positive impact is more pronounced in LiOH-derived samples, where coating mitigates the otherwise poor cycling performance of the pristine NMC811H. The superiority of the T-based coatings indicates that

precursor residuals play a key role in stability. While full dynamic evolution of the interface requires further investigations like long-term EIS or rate capability tests, the present dQ/dU peak data confirms an improvement in structural capacity retention and voltage stability [28,29].

Overall, the results confirm that: (a) Li_2CO_3-based NMC811 (NMC811C) offers better intrinsic cycling performance than LiOH-based NMC811 (NMC811H); (b) $LiNbO_3$ coating, particularly using T-precursor, significantly enhances the initial capacity and reduces degradation; (c) proper selection of both lithium precursor and niobium coating precursor is critical for optimizing NMC811 cathode performance; (d) aqueous Nb-based coating attempts (NbAmOx route) on NMC811C resulted in poor electrochemical performance, indicating that nickel-rich self-synthesized NMC materials are also highly sensitive to water and require the ethanol-based H_2O_2 coating route for successful modification.

It is worth mentioning, that we are aware that the self-synthesized NMC811C and NMC811H materials leave room for improvement, for example, a longer initial calcination time might reduce cation mixing more effectively, potentially eliminating the need for an additional 350 °C treatment in the case of NMC811H. However, optimization of the synthesis process was not the focus of this study. The goal here was not to produce a "perfect" material, but rather to apply a consistent coating process and assess the contribution of the coating itself. This approach allows a fair comparison between coated and uncoated samples, regardless of the initial quality of the material. While commercial materials like Ni82 are likely already optimized (though their synthesis details are not disclosed), our aim was also to use well-defined, reproducible in-house materials to investigate the effect of two different Nb precursors. Finally, we acknowledge that deeper insights into the observed electrochemical behavior will require further advanced characterization, which is beyond the scope of this work and will be addressed in future studies.

3.6. Role of Nb-ethoxide precursor purity

To investigate the origin of the performance differences observed between samples coated using two different niobium ethoxide precursors, X-ray photoelectron spectroscopy (XPS) was performed on the decomposition products of each precursor. Upon exposure to air, the liquid niobium ethoxide rapidly decomposed into a white powder, which was collected and analyzed.

The XPS spectra of the powder obtained from the T-precursor revealed the presence of two weak peaks corresponding to silicon (Si) and fluorine (F), indicating minor impurities or residuals from the precursor synthesis or packaging process. In the powder derived from the A-precursor, the corresponding Si and F signals were only barely detectable, suggesting markedly lower impurity levels (Fig. S8). While at first glance these impurities may seem undesirable, their presence may in fact contribute positively to the observed electrochemical behavior. The superior initial capacity, cycling stability and specific capacity retention of the $LiNbO_3$-coated NMC811 samples using the T-precursor could be partially attributed to these trace elements. Possible explanations include:

(a) Surface passivation effects: Fluorine plays a key role in stabilizing the cathode interface. It promotes the formation of a robust, thin cathode-electrolyte interphase (CEI), which is distinct from the solid-electrolyte interphase (SEI) traditionally formed on the anode side. This well-defined fluorinated CEI enhances structural stability at high operating voltages by suppressing continuous electrolyte oxidation and parasitic side reactions [30–32];
(b) Silicon-related compounds: Silicon oxides or silicates may contribute to additional surface passivation or alter the coating morphology, enhancing the mechanical and chemical stability of the coating layer [33,34];
(c) Modified coating chemistry: The presence of Si and F may subtly influence the decomposition pathways or crystallization behavior of the $LiNbO_3$ layer during thermal treatment, possibly affecting ionic and/or electronic conductivity, interface adhesion, or coating uniformity [35,36].

The last explanation is the most plausible, because the amounts of F and Si are too small for explanations (a) and (b) to be realistic. It is also important to note that $LiNbO_3$ is an electronic insulator, and, for example, partial substitution of oxygen ions by fluoride ions would increase the electronic conductivity, as Nb^{5+} would be partially reduced, introducing mixed-valence states/partially filled d-orbitals. We note that these mechanisms remain hypothetical. The trace amounts of Si and F on the final coated active materials were below the detection limit of our laboratory XPS. However, the correlation between these precursor residuals and the improved electrochemical stability is reproducible, and similar adjustments to electronic conductivity via fluoride substitution are known in literature.

Although the exact mechanism by which these impurities influence performance requires further investigation, the correlation between their presence (as identified by XPS) and the enhanced electrochemical performance of the T-derived coatings is noteworthy. These findings highlight the importance of precursor purity and composition, even at trace levels, in determining the final electrochemical behavior of surface-modified cathode materials.

4. Conclusions

This work demonstrates that the H_2O_2-assisted $LiNbO_3$ coating procedure, previously optimized for spinel cathodes, is also highly effective for layered oxide materials. Comparative studies between commercial and self-synthesized nickel-rich layered oxides clearly show that the unexpectedly poor performance of coated commercial material is not attributed to the coating chemistry itself, but rather to the unknown processing history of the commercial powder, which likely involves prior surface treatments that hinder new coating reactions. In contrast, self-synthesized layered oxides provided a reproducible and well-defined platform for studying surface modifications. Both carbonate- and hydroxide-based syntheses yielded phase-pure materials, but the Li_2CO_3-derived NMC811 consistently exhibited superior electrochemical stability and specific capacity, underscoring the strong influence of lithium precursor chemistry on bulk and interfacial properties. Application of $LiNbO_3$ coatings via the H_2O_2-assisted route, followed by mild calcination at 350 °C, significantly enhanced the cycling stability of both NMC811 variants.

XPS analysis revealed minor trace Si and F species in the T-derived precursor, suggesting that even minor impurities or residual elements in precursor solutions can beneficially influence interfacial stability and electrochemical performance. These findings highlight the sensitivity of Ni-rich layered oxides to surface chemistry and demonstrate that for self-synthesized layered oxides the H_2O_2-assisted coating approach is broadly applicable and intrinsically benign.

In summary, the H_2O_2-based $LiNbO_3$ coating method represents a robust and versatile surface modification strategy for both spinel and layered oxide cathodes. However, reliable interpretation and optimization require the use of self-synthesized, compositionally well-characterized materials with known processing histories. Such control enables the establishment of reproducible correlations between synthesis, surface chemistry, and electrochemical behavior, ultimately guiding the rational design of durable high-energy cathodes.

CRediT authorship contribution statement

Valeriu Mereacre: Writing – review & editing, Writing – original draft, Visualization, Validation, Methodology, Investigation, Formal analysis, Data curation, Conceptualization. **Yiran Guo:** Writing –

original draft, Investigation, Formal analysis. **Ruochen Xu:** Writing – original draft, Visualization, Validation, Software, Investigation, Formal analysis. **Markus Weinmann:** Writing – original draft, Resources, Data curation. **Ralph D. Otterstedt:** Writing – original draft, Validation, Resources, Data curation. **Joachim R. Binder:** Writing – original draft, Validation, Supervision, Resources, Project administration, Funding acquisition, Data curation, Conceptualization.

Declaration of competing interest

The authors declare that they have no known competing financial interests or personal relationships that could have appeared to influence the work reported in this paper.

Acknowledgments

Funding from the Bundesministerium für Bildung und Forschung (BMBF) within the FESTBATT cluster of competence (projects 03XP0433A) is gratefully acknowledged. We also thank Dr. Thomas Bergfeldt for support with ICP-OES analysis and Vanessa Trouillet for the XPS measurements.

Appendix A. Supplementary data

Supplementary data to this article can be found online at https://doi.org/10.1016/j.jelechem.2026.120693.

References

[1] L. Wang, J. Wang, Y. Lu, S. Fang, C. Yang, X. Wu, Y. Xiao, Y. Wang, S. Chou, S. Chen, Chem. Soc. Rev. 54 (2025) 4419–4467.
[2] H. Chen, X. Xia, J. Ma, ChemSusChem 17 (2024) e202401120.
[3] F. Xin, H. Zhou, Y. Zong, M. Zuba, Y. Chen, N.A. Chernova, J. Bai, B. Pei, A. Goel, J. Rana, F. Wang, K. An, L.F.J. Piper, G. Zhou, M.S. Whittingham, ACS Energy Lett. 6 (2021) 1377–1382.
[4] F. Xin, H. Zhou, J. Bai, F. Wang, M.S. Whittingham, J. Phys. Chem. Lett. 12 (2021) 7908–7913.
[5] T. Teng, L. Xiao, J. Zheng, D. Wen, H. Chen, Y. Zhu, Ceram. Int. 48 (2022) 8680–8688.
[6] L. Zhang, L. Xiao, J. Zheng, H. Wang, H. Chen, Y. Zhu, J. Electrochem. Soc. 168 (2021) 110528.
[7] G. Hu, Y. Tao, Y. Lu, J. Fan, L. Li, J. Xia, Y. Huang, Z. Zhang, H. Su, Y. Cao, ChemElectroChem 6 (2019) 4773–4780.
[8] B. Wang, H. Zhao, F. Cai, Z. Liu, G. Yang, X. Qin, K. Świerczek, Electrochim. Acta 403 (2022) 139636.
[9] R. Zhao, J. Liang, J. Huang, R. Zeng, J. Zhang, H. Chen, G. Shi, J. Alloys Compd. 724 (2017) 1109–1116.
[10] V. Mereacre, P. Stüble, A. Ghamlouche, J.R. Binder, Nanomaterials 11 (2021) 548–560.
[11] V. Mereacre, N. Bohn, P. Stüble, L. Pfaffmann, J.R. Binder, ACS Appl. Energy Mater. 4 (2021) 4271–4276.
[12] V. Mereacre, P. Stüble, V. Trouillet, S. Ahmed, K. Volz, J.R. Binder, Adv. Mater. Interfaces 10 (2022) 2201324.
[13] D. Kitsche, F. Strauss, Y. Tang, N. Bartnick, A.-Y. Kim, Y. Ma, C. Kübel, J. Janek, T. Brezesinski, Batteries Supercaps 5 (2022) e202100397.
[14] W. Sun, M. Xie, X. Shi, L. Zhang, Mater. Res. Bull. 61 (2015) 287–291.
[15] G. Lu, W. Peng, Y. Zhang, X. Wang, X. Shi, D. Song, H. Zhang, L. Zhang, Electrochim. Acta 368 (2021) 137639.
[16] A. van Bommel, J.R. Dahn, Chem. Mater. 21 (2009) 1500–1503.
[17] T. Wang, Y. Xu, H. Ye, S. Chen, Q. Zhang, J. Zhao, S. Zhang, X. Xia, J. Tu, Small 16 (2020) 2002578.
[18] M. Almazrouei, F. Hasan, A.A. Elamin, A.A.A. lkaabi, E.H. Alhammadi, H. A. Alnaqbi, A.S. Alnuaimi, A.M.K. Esawi, S.S. Faraj, S.K. Amer, Mater. Today Proc. 62 (2022) 5699–5704.
[19] F.I. Saaid, M.M. Rahman, M.M. Hossain, Electrochim. Acta 307 (2019) 115–123.
[20] J. Haust, Y. Guo, J. Belz, S. Ahmed, N. Adeli, F. Hüppe, L.C. Erhard, V. Mereacre, J. Rohrer, A.-L. Hansen, H. Ehrenberg, K. Albe, J.R. Binder, K. Volz, Adv. Mater. Interfaces 12 (17) (2025) e00590, https://doi.org/10.1002/admi.202500590.
[21] F. Xin, H. Zhou, X. Chen, M. Zuba, N. Chernova, G. Zhou, M.S. Whittingham, ACS Appl. Mater. Interfaces 11 (2019) 34889–34894.
[22] B. Ying, J.R. Fitzpatrick, Z. Teng, T. Chen, T.W.B. Lo, V. Siozios, C.A. Murray, H.E. A. Brand, S. Day, C.C. Tang, R.S. Weatherup, M. Merz, P. Nagel, S. Schuppler, M. Winter, K. Kleiner, Chem. Mater. 35 (2023) 1514–1526.
[23] J. Zhu, G. Chen, J. Mater. Chem. A 7 (2019) 5463–5474.
[24] T. Li, X.-Z. Yuan, L. Zhang, D. Song, K. Shi, C. Bock, Electrochem. Energy Rev. 3 (2020) 43–80.
[25] R. Ruedl, M.A. Ulherr, E. Trevisanello, S. Schröder, A. Henss, J. Janek, J. Electrochem. Soc. 169 (2022) 070531.
[26] X. Sun, S. Hori, Y. Li, Y. Yamada, K. Suzuki, M. Hirayama, R. Kanno, J. Mater. Chem. A 9 (2021) 4117–4125.
[27] Y. Zhou, Z. Hu, Y. Huang, Y. Wu, Z. Hong, J. Alloys Compd. 888 (2021) 161584.
[28] H. Shi, J. Wu, F. Zheng, M. Su, A. Naveed, P. Zhang, D. Wang, D. Wang, H. Wang, S. Hong, Y. Liu, Y. Zhou, Y. Liu, Energy Storage Mater. 89 (2026) 105276.
[29] H. Shi, J. Zheng, T. Wan, H. Wang, Z. Wen, F. Zheng, M. Su, A. Dou, Y. Zhou, A. Naveed, P. Zhang, H. Wang, R. Guo, Y. Liu, D. Chu, J. Energy Chem. 101 (2025) 392–401.
[30] K. Xu, Chem. Rev. 114 (2014) 11503–11618.
[31] R. Jung, M. Metzger, F. Maglia, C. Stinner, H.A. Gasteiger, J. Electrochem. Soc. 164 (2017) A1361–A1377.
[32] J. Park, B. Xu, R.E. White, J. Power Sources 437 (2019) 226923.
[33] D. Mohanty, S. Kalnaus, J. Li, E.A. Payzant, D.L. Wood, C. Daniel, J. Power Sources 245 (2014) 291–298.
[34] H. Lee, P. Yan, J.J. Vajo, S. Litzelman, C. Wang, ACS Appl. Mater. Interfaces 7 (2015) 2404–2412.
[35] Y. Wang, J. Li, Y. Gong, W. Liu, S. Xu, Y. Li, Adv. Energy Mater. 11 (2021) 2003322.
[36] X. Zhang, X.-B. Cheng, C.-Z. Zhao, Q. Zhang, Adv. Funct. Mater. 30 (2020) 1909895.